# Molecular Aggregate Photophysics beyond the Kasha Model: Novel Design Principles for Organic Materials

Nicholas J. Hestand and Frank C. Spano*

Department of Chemistry Temple University Philadelphia, Pennsylvania 19122, United States

CONSPECTUS: The transport and photophysical properties of organic molecular aggregates, films, and crystals continue to receive widespread attention, driven mainly by expanding commercial applications involving display and wearable technologies as well as the promise of efficient, large-area solar cells. The main blueprint for understanding how molecular packing impacts photophysical properties was drafted over five decades ago by Michael Kasha. Kasha showed that the Coulombic coupling between two molecules, as determined by the alignment of their transition dipoles, induces energetic shifts in the main absorption spectral peak and changes in the radiative decay rate when compared to uncoupled molecules. In H-aggregates, the transition dipole moments align "side-by-side" leading to a spectral blue-shift and

suppressed radiative decay rate, while in J-aggregates, the transition dipole moments align "head-to-tail" leading to a spectral red-shift and an enhanced radiative decay rate. Although many examples of H- and J-aggregates have been discovered, there are also many "unconventional" aggregates, which are not understood within the confines of Kasha's theory. Examples include nanopillars of 7,8,15,16-tetraazaterrylene, as well as several perylene-based dyes, which exhibit so-called H- to J-aggregate transformations. Such aggregates are typically characterized by significant wave function overlap between neighboring molecular orbitals as a result of small (~4 Å) intermolecular distances, such as those found in rylene π-stacks and oligoacene herringbone lattices. Wave function overlap facilitates charge-transfer which creates an effective short-range exciton coupling that can also induce J- or H-aggregate behavior, depending on the sign.

Unlike Coulomb coupling, short-range coupling is extremely sensitive to small (sub-Å) transverse displacements between neighboring chromophores. For perylene chromophores, the sign of the short-range coupling changes several times as two molecules are "slipped" from a "side-by-side" to "head-to-tail" configuration, in marked contrast to the sign of the Coulomb coupling, which changes only once. Such sensitivity allows J- to H-aggregate interconversions over distances several times smaller than those predicted by Kasha's theory. Moreover, since the *total* coupling drives exciton transport and photophysical properties, interference between the short- and long-range (Coulomb) couplings, as manifest by their relative signs and magnitudes, gives rise to a host of new aggregate types, referred to as HH, HJ, JH, and JJ aggregates, with distinct photophysical properties. An extreme example is the "null" HJ-aggregate in which total destructive interference leads to absorption line shapes practically identical to uncoupled molecules. Moreover, the severely compromised exciton bandwidth effectively shuts down energy transport. Most importantly, the new aggregates types described herein can be exploited for electronic materials design. For example, the enhanced exciton bandwidth and weakly emissive properties of HH-aggregates make them ideal candidates for solar cell absorbers, while the enhanced charge mobility and strong emissive behavior of JJ-aggregates makes them excellent candidates for light-emitting diodes.
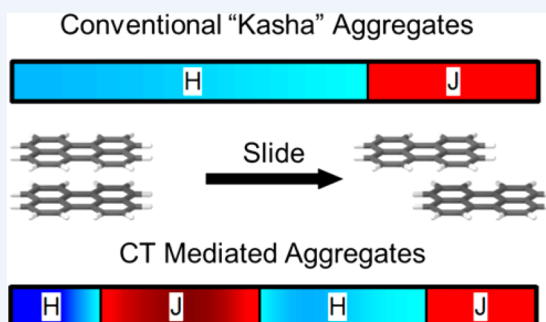
I. INTRODUCTION

The expanding interest in conjugated organic materials for applications in display technology[1−4] and photovoltaics[3−5] has motivated many investigations into the nature of electronic excitations in organic molecular assemblies.[4−13] In the aggregated or crystalline phase, intermolecular interactions, which strongly depend on the packing arrangement, play a key role in determining the photophysical response as well as the nature of energy and charge transport. Perhaps the most significant breakthrough linking packing geometry and photophysical properties was achieved by Michael Kasha over 5 decades ago.[14−16] Kasha showed that relative to isolated monomers molecular dimers stacked "side-by-side" exhibit a blue-shifted absorption maximum and suppressed radiative

decay rate while dimers stacked "head-to-tail" exhibit a red-shifted absorption maximum and enhanced radiative decay rate. The former became known as H-aggregates and the latter as J-aggregates. Throughout the years, many examples of H- and J-aggregation have been discovered,[17−22] exhibiting geometries ranging from simple dimers[18] to macroscopic nanotubes.[21] The rylene family of dyes are particularly interesting, as they have been observed to form both H- and J-aggregates.[22]

In Kasha's model, the geometries that lead to J- and H-aggregates are predicated on long-range Coulomb coupling alone. However, in certain packing arrangements such as π-

stacks, neighboring molecules are close enough (∼3.5 Å) to allow for significant wave function overlap and the emergence of short-range interactions.[23,24] As we show below, such interactions also promote J- and H-aggregate behavior, although with significantly different spatial dependencies than those associated with Kasha's H- and J-aggregates. Importantly, the magnitude of the short-range coupling can be comparable to or even exceed the Coulomb coupling, thereby enabling pronounced interference effects, which render the conventional geometric classification scheme of H- and J-aggregates incomplete at best. The model presented in this Account allows one to better appreciate the novel photophysics inherent to many π-stacked systems including 7,8,15,16-tetraazaterrylene (TAT) nanopillars,[25−27] where the interference between long- and short-range couplings can be observed directly from vibronic signatures present in the absorption line shape, and the so-called H- to J-aggregate transformation induced by slight packing changes in several perylene bisimide aggregates.[28−30] The interference between long and short-range couplings can also form the basis for optimizing exciton transport[31] and luminescence in organic materials.

II. NATURE OF THE EXCITONIC COUPLING

The interplay between the short- and long-range interactions is readily appreciated within a simple model based on a disorder-free linear π-stack containing N chromophores with one molecule per unit cell (see Figure 1). Each chromophore is
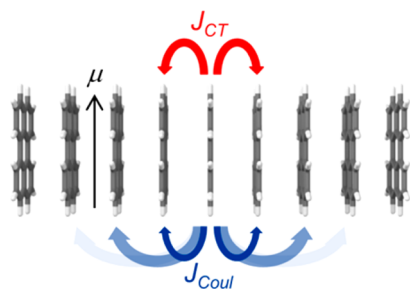

Figure 1. Model perylene π-stack showing short-range charge-transfer (CT)-mediated interactions, J_{CT}, and long-range Coulomb interactions, for which J_{Coul} is the nearest-neighbor.

characterized by an electronic $S_0 \rightarrow S_1$ (HOMO−LUMO) transition with energy E_{S_1}, and transition dipole moment $\boldsymbol{\mu}$, both of which are independent of the chromophore's position. As shown by Harcourt et al.,[23] the excitonic interactions can be divided into long-range Coulombic interactions and short-range exchange (Dexter[24]) and superexchange interactions deriving from wave function overlap. A similar division can be made for covalently bound chromophores.[32]

Retaining only the Coulombic interactions leads to Kasha's exciton model, which is summarized in Figure 2. The Coulomb coupling between any two chromophores arises from the interaction between their transition charge distributions and is often expressed using the point-dipole approximation,

$$J_{Coul} \approx \frac{\mu^2(1 - 3\cos^2\theta)}{4\pi\varepsilon R^3} \quad (1)$$

where R is the intermolecular distance between mass centers, θ is the angle between $\boldsymbol{\mu}$ and R, and ε is the optical dielectric constant of the medium, see Figure 2a. Intermolecular coupling leads to delocalized (Frenkel) excitons, which assuming
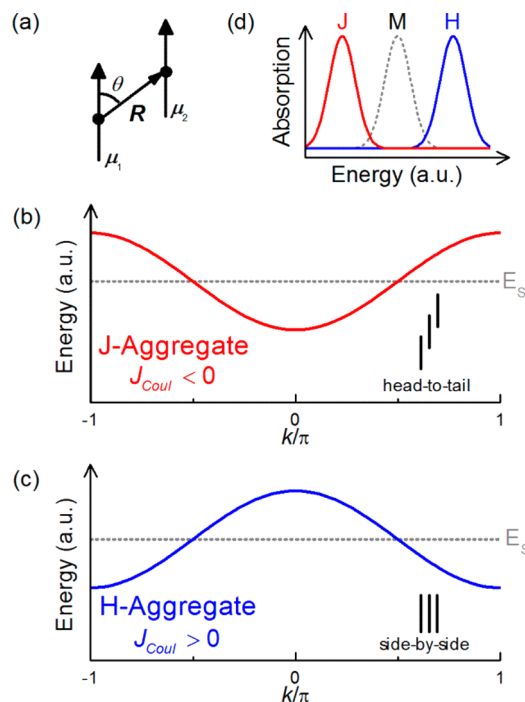

Figure 2. (a) Transition dipole geometry for evaluating the Coulombic coupling under the point dipole approximation. Exciton energy bands of Kasha (b) J-aggregates and (c) H-aggregates from eq 3. In J- and H-aggregates, the optically allowed exciton ($k = 0$) resides at the bottom and top of the band, respectively. The packing geometries associated with each aggregate type are shown as insets. (d) Ideal absorption spectra for J- and H-aggregates.

periodic boundary conditions can be expressed according to their wave vector, k, as[33]

$$|k\rangle = \frac{1}{\sqrt{N}} \sum_n e^{ikn}|n\rangle \qquad k = 0, \pm2\pi/N, \pm4\pi/N, ...\pi \quad (2)$$

where $|n\rangle$ denotes a HOMO−LUMO excitation on the nth chromophore. When the coupling is limited to nearest neighbors, the energy of the exciton with wave vector k is

$$E_F(k) = E_{S_1} + 2J_{Coul}\cos k \quad (3)$$

Figures 2b and 2c show plots of the band dispersion, $E_F(k)$, for negative and positive values of J_{Coul} corresponding to conventional Kasha J-aggregates and H-aggregates, respectively. As only the nodeless ($k = 0$) exciton carries oscillator strength, the transition energy is lower than the monomer energy (E_{S_1}) when J_{Coul} is negative and higher in energy when J_{Coul} is positive. This is manifest photophysically as an aggregation-induced red-shift and blue-shift, respectively, in the optical absorption spectrum of J-aggregates and H-aggregates, see Figure 2d.

The geometric embodiment of J- and H-aggregates derives from eq 1. Hence, "head-to-tail" orientations ($\theta \approx 0$) give rise to J-aggregates, while "side-by-side" orientations ($\theta \approx \pi/2$) lead to H-aggregates. More sophisticated treatments of the Coulomb coupling using atomic transition charge densities give a qualitatively similar picture.[34−36]

In contrast to J_{Coul}, the superexchange interaction derives from wave function overlap between neighboring molecules and therefore diminishes exponentially with distance. LUMO−

LUMO and HOMO–HOMO overlap, which can be substantial in π-stacks due to the close nearest-neighbor contacts ($\sim$3.5 Å), facilitates the dissociation of local excitations ($|n\rangle$) into charge-transfer (CT) states[37−40] where electrons and holes reside on neighboring chromophores, see Figure 3. To a
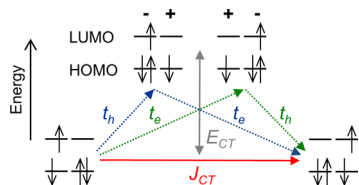

Figure 3. Energy level diagram depicting charge transfer between neighboring chromophores. J_{CT} results from the sum of the blue and green virtual two-step pathways.

good approximation, the dissociation integrals for electrons and holes are equal to the electron and hole transfer integrals, t_e and t_h, respectively.[41] As shown by Kazmeier and Hoffman,[42] t_h and t_e are hypersensitive to the transverse registry of neighboring chromophores, as they derive from the overlap between neighboring HOMOs and LUMOs, respectively. This sensitivity is illustrated in Figure 4a–d for a perylene dimer. Since the conduction and valence bandwidths directly scale with $|t_e|$ and $|t_h|$, respectively, the optical gap is also very sensitive to intermolecular orientation, leading to the broad range of pigment colors exhibited by crystalline perylene derivatives.[40,42]

So long as the diabatic Frenkel and CT exciton states are energetically well-separated, the CT state can be considered virtual. In this perturbative limit, charge transfer gives rise to an effective short-range exciton coupling,[23,43,44]

$$J_{CT} = -2\frac{t_e t_h}{E_{CT} - E_{S_1}} \qquad |E_{CT} - E_{S_1}| \gg |J_{Coul}|, |t_e|, |t_h|$$

(4)

where E_{CT} is the energy of the CT exciton. As depicted in Figure 3, the CT mediated superexchange coupling arises from the transfer of an electron and hole (and vice versa) through the virtual CT intermediate state. In contrast, the Dexter exchange integral leads to direct energy transfer but was shown by Scholes et al.[23] to be insignificant relative to J_{CT} in π-stacked chromophores.

According to eq 4, J_{CT} can be positive or negative depending on the signs of $t_e t_h$ and $E_{CT} - E_{S_1}$. Assuming the latter to be positive[45] results in J-like coupling when $t_e t_h > 0$ and H-like coupling when $t_e t_h < 0$. (The J- and H-aggregate behaviors are interchanged when $E_{CT} < E_{S_1}$). The dependence of J_{CT} on the product $t_e t_h$ makes the short-range coupling extremely sensitive to small transverse displacements between neighboring chromophores, as demonstrated for perylene in Figure 4e; notably J_{CT} is far more sensitive than J_{Coul} (compare Figures 4e and 4f). The role that the HOMO and LUMO nodal patterns play in determining the signs of t_h and t_e[41] can be appreciated from Figure 4a–d. When slipped along the long molecular axis t_e does not change sign because the perylene LUMO contains no longitudinal nodes (i.e., there are no nodes crossing the dotted line in Figure 4d). Comparatively, t_h will change sign three times as a consequence of the three nodes encountered along the long molecular axis in the perylene HOMO. These
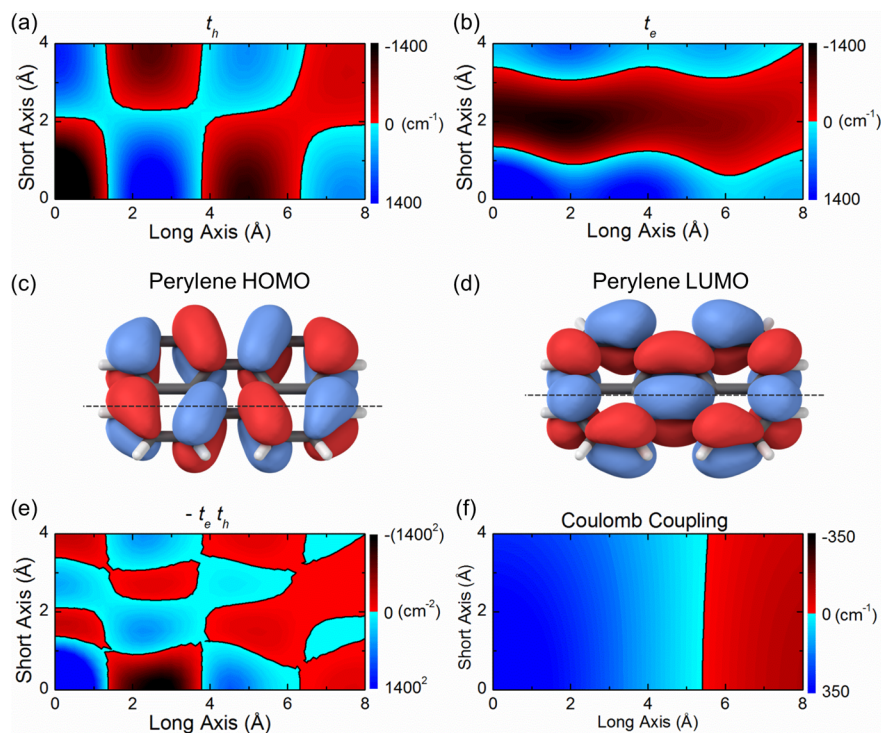

Figure 4. (a) t_h and (b) t_e within a π-stacked perylene dimer (3.5 Å π-stacking distance) as a function of transverse displacement, evaluated from density functional theory (DFT) calculated energy level splittings. The DFT calculated (c) HOMO and (d) LUMO of perylene. (e) The product, $t_e t_h$ ($\propto J_{CT}$), and (f) the unscreened Coulomb coupling as a function of transverse displacement, evaluated using time-dependent DFT calculated atomic transition charge densities. Red (blue) regions correspond to a J- (H−) type interaction. All DFT calculations use the B3LYP functional and cc-pVDZ basis. The sign convention for t_e and t_h is based on symmetry operations under which the dimer transition dipole moment is symmetric.[43]

sign changes have a profound effect on the J/H-like nature of J_{CT} and the overall photophysical properties. We emphasize that the spatial dependences of t_h and t_e depend on the conjugation topology, with significant differences existing between perylenes,[40,42,44] oligothiophenes,[8,43] and oliogoacenes.[10]

In the perturbative limit, the two coupling sources are additive, as is evident in the effective Frenkel exciton Hamiltonian[43,44]

$$H_{ex} = E_{S_1} + \Delta_{CT} + \sum_n (J_{Coul} + J_{CT})\{|n\rangle\langle n+1| + |n+1\rangle\langle n|\}$$

$$|E_{CT} - E_{S_1}| \gg |t_e|, |t_h| \tag{5}$$

where electron/hole recombination results in a self-energy correction given by

$$\Delta_{CT} = -2\frac{t_e^2 + t_h^2}{E_{CT} - E_{S_1}} \tag{6}$$

Equation 5 shows that the net coupling derives from an interference between J_{Coul} and J_{CT}, which is most pronounced when they have similar magnitudes. The geometric dependence of the net coupling can be appreciated by comparing Figures 4e and 4f for a perylene dimer. Starting from an eclipsed conformation, a longitudinal slip of about 5.5 Å along the long-axis is required to induce a sign change (signaling an H- to J-aggregate transformation) in J_{Coul}. In marked contrast J_{CT} ($\propto -t_e t_h$) changes sign almost three times over the same interval, with the first change occurring at approximately 1.6 Å, allowing for a range of geometries hosting constructive or destructive interferences between J_{Coul} and J_{CT}. Furthermore, when $|J_{CT}| > |J_{Coul}|$, it is possible to have H- and J-aggregate behavior at unconventional (non-Kasha) packing geometries, for example, slightly slipped "side-by-side" J-aggregates. For a quantitative description, one must also account for changes in the Coulombic component of the CT energy, which was recently shown to be small, <300 cm^{-1} in terrylene when slipping by almost 8 Å.[46] Moreover, interferences are also impacted by thermal fluctuations.[47]

The results described above are strictly applicable in the perturbative limit where CT states are far removed energetically from the Frenkel states. When this is not true, resonance effects between Frenkel and CT excitons lead to additional complexities. Moreover, the competition between J_{Coul} and J_{CT} takes place in the presence of strong electronic–nuclear coupling involving the ubiquitous ring/vinyl stretching mode typical of most π-conjugated molecules. In the perturbative limit, the coupling is readily accounted for by adding vibronic coupling terms to the Hamiltonian in eq 5, giving rise to vibronic spectral signatures, which more clearly resolve H- vs J-aggregation.[13] In the most general case, Holstein-style Hamiltonians, which explicitly include CT states, are necessary.[31,44] In the following sections, we investigate the impact of the competition between J_{Coul} and J_{CT} on the photophysical behaviors of several rylene-based systems under a variety of conditions, ultimately presenting a novel set of design principles for organic electronics.

III. CHARGE-TRANSFER H- AND J-AGGREGATES

In this section, we show how Frenkel/CT mixing[37−40] can induce H- and J-aggregate behavior in the absence of Coulomb coupling. Such a situation may seem unnatural but is actually a

fairly accurate description for tetracene and pentacene crystals, where the Coulomb coupling within the lowest energy exciton band is compromised due to a weakly allowed, short-axis polarized $S_0 \rightarrow S_1$ transition, resulting in photophysics dominated by strong Frenkel/CT mixing.[48] Aggregates characterized by $|J_{CT}| \gg |J_{Coul}|$ are referred to as charge-transfer J- and H-aggregates.

In what follows, we assume that CT states are limited to nearest neighbors, a good approximation for the strongly bound electron/hole pairs characteristic of organic materials. When t_e and t_h are both zero, the excited states are either pure Frenkel excitons, as described by eq 2, or pure CT excitons. The latter can also be described as delocalized excitations but with two degenerate CT excitons per wave vector k. All $2N$ CT states can be expressed as

$$|k, \pm\rangle = \frac{1}{\sqrt{2N}} \sum_n \{e^{ikn+i\theta(k)}|n, n+1\rangle$$

$$\pm e^{ikn-i\theta(k)}|n, n-1\rangle\} \tag{7}$$

Here, $|n, n'\rangle$ represents a local CT excitation with a hole residing on chromophore n and an electron on n' and $e^{i\theta(k)} = z/|z|$, with $z \equiv t_e + t_h e^{ik}$. The phase factor simplifies the form of the coupling to Frenkel excitons (see eq 8).[49] The two (diabatic) CT bands defined by eq 7 are dispersionless (flat) with energy $E_{CT} = I_P + E_A - e^2/(4\pi\varepsilon_S R) + P$. Here, I_P is the molecular ionization potential, E_A is the electron affinity, P is the polarization energy, and $e^2/(4\pi\varepsilon_S R)$ is the electrostatic binding energy. In what follows, we neglect the oscillator strength of the $|k = 0, +\rangle$ exciton as it is typically much smaller than that of the $k = 0$ Frenkel exciton.[40]

The Frenkel excitons in eq 2 and CT excitons in eq 7 are referred to as diabatic because they are not yet coupled to each other. Coupling arises from the ionization of a Frenkel exciton, $|k\rangle$, into the CT state, $|k, +\rangle$ dictated by the matrix element,

$$\langle k|H|k, +\rangle = \sqrt{2}|t_e + t_h e^{ik}| \tag{8}$$

The CT states $|k, -\rangle$ (ignored from here on) remain uncoupled. Hence, the eigenspectrum is readily obtained by diagonalizing N 2×2 matrices (one per k) resulting in the general dispersion relationship for the lower and upper mixed Frenkel/CT bands,[44]

$$E_\pm(k) = \frac{E_{CT} + E_F(k)}{2}$$

$$\pm \sqrt{\left(\frac{E_{CT} - E_F(k)}{2}\right)^2 + 2(t_e^2 + t_h^2 + 2t_e t_h \cos k)} \tag{9}$$

For the remainder of this section, we consider the limit $J_{Coul} = 0$ and take $E_{CT} > E_{S_1}$. In this case, the perturbative limit of eq 9 applies whenever $E_{CT} - E_{S_1} \gg |t_e|, |t_h|$, whereupon eq 9 reduces to

$$E_-(k) = E_{S_1} + \Delta_{CT} + 2J_{CT} \cos k \tag{10a}$$

$$E_+(k) = E_{CT} - \Delta_{CT} - 2J_{CT} \cos k \tag{10b}$$

For $E_{CT} \gg E_{S_1}$, the lower exciton band ($E_-(k)$) is almost entirely Frenkel-like and therefore contains the bulk of the oscillator strength. The upper band, dominated by the CT component, remains dark. In this case eq 10a can be derived directly from the effective Hamiltonian in eq 5.
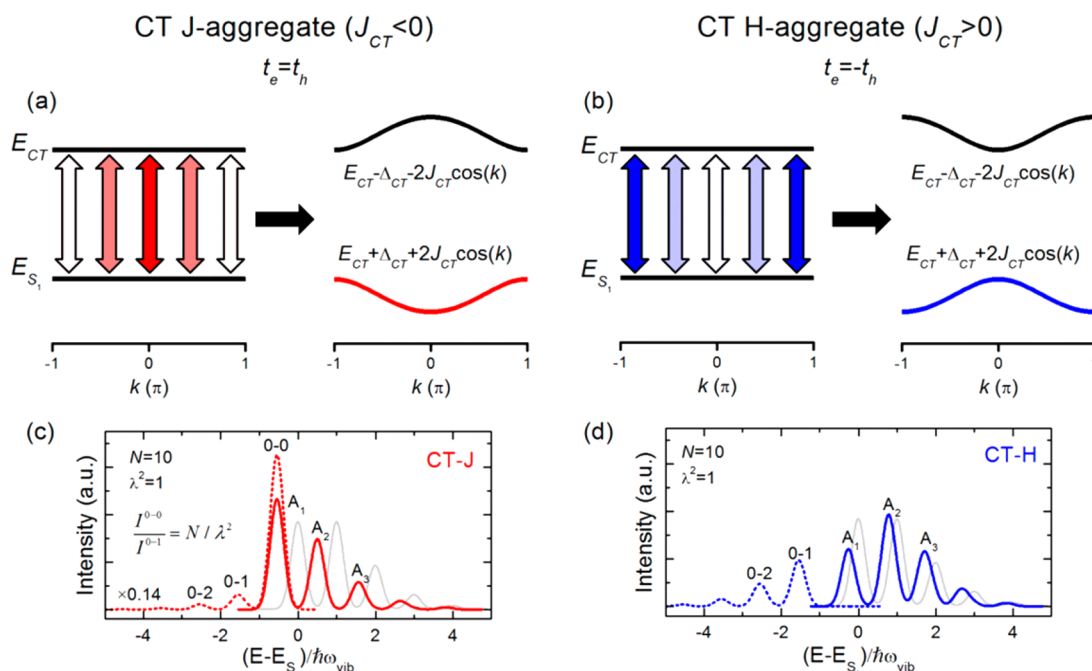
Figure 5. Energy level diagrams depicting the interaction between the diabatic CT band and the (flat) Frenkel band in (a) CT J-aggregates and (b) CT H-aggregates with $|t_e| = |t_h|$. The magnitude of the k-dependent Frenkel/CT coupling is illustrated by the intensity of the red and blue shading in panels (a) and (b), respectively, see eq 8. The corresponding absorption and PL spectra are shown in panels (c) and (d) as the solid and dotted colored lines, respectively. Both cases consider a disorder-free π-stack at $T = 0$ K with $E_{CT} - E_{S_1} = 10$, $\lambda^2 = 2\lambda_\pm^2 = 1$, and $J_{Coul} = 0$. All energies are in units of $\hbar\omega_{vib}(=1400$ cm^{-1}). The monomer absorption spectra are shown in gray. The monomer PL spectrum (not shown) is the mirror image of the absorption spectrum.

Figure 5a demonstrates how the band structure develops in a CT J-aggregate when both diabatic bands are flat. Here, t_e and t_h are taken to have the same sign ($J_{CT} < 0$) thereby inducing positive curvature in $E_-(k)$. Notably, the optically bright state ($k = 0$) lies at the band bottom (below E_{S_1}) leading to a red-shifted absorption peak and superradiant emission, both signatures of J-aggregation. *The geometries of such CT-mediated J-aggregates, however, can be entirely different from conventional Kasha H- and J-aggregates.* Figure 4e illustrates how the geometries promoting CT J-aggregation in perylene π-stacks (red regions) differ from those defining conventional Kasha J-aggregates in Figure 4f.

Figure 5b demonstrates the band structure of a CT H-aggregate where t_e and t_h have opposite signs, $t_e = -t_h$ ($J_{CT} > 0$). In this case, a negative curvature is induced in the lowest band creating H-aggregate photophysics. The optically bright state now resides at the top of the (lower) band so that radiation from the band-bottom is suppressed, consistent with the behavior of conventional Kasha H-aggregates. Curiously though, the bright exciton is not blue-shifted from the monomer due to an exact cancellation between the CT-induced red-shift, Δ_{CT}, and the excitonic blue-shift, $2J_{CT}$ (at $k = 0$) (see eqs 4 and 6). The lack of an excitonic blue-shift represents the only departure from conventional Kasha H-aggregate photophysics. As for CT J-aggregates, the geometries of CT H-aggregates can differ markedly from those of Kasha H-aggregates (compare the blue regions of Figures 4e and 4f).

The photophysical behavior of CT J- and H-aggregates can also be analyzed with respect to the vibronic signatures outlined in ref 13 for conventional Kasha aggregates. Vibronic coupling arises from the vinyl stretching mode and is driven by a shifted excited state (S_1) nuclear potential relative to the ground state (S_0) potential. For a single molecule the shift leads to the usual vibronic progressions with the mth peak intensity governed by $\exp(-\lambda^2)\lambda^{2m}/m!$, where λ^2 is the Huang–Rhys (HR) factor. In Kasha aggregates, the vibronic progression is distorted; the ratio of the oscillator strengths of the first two vibronic peaks in the absorption spectrum, A_1/A_2, reflects the strength of the exciton coupling and is enhanced relative to the isolated monomer in J-aggregates and suppressed relative to the isolated monomer in H-aggregates. The dichotomy extends to the photoluminescence (PL) spectrum where the 0−0/0−1 ratio is strongly enhanced relative to the monomer in J-aggregates and suppressed relative to the monomer in H-aggregates. Figures 5c and 5d show the associated absorption and PL spectra for the CT aggregates in Figures 5a and 5b, after allowing for local vibronic coupling. In Figure 5, we assume $\lambda^2 = 1$ so that for a single molecule the first two vibronic peaks in the absorption spectrum have equal intensity (see the gray-colored spectrum). Notably, *the vibronic signatures of CT J- and H-aggregates are identical to those displayed by conventional Kasha aggregates.*[13] Note that we have neglected possible excimer contributions to the PL,[45] which is a good approximation for some rylenes such as TAT, which show no evidence of excimer emission.[25,26]

To demonstrate that CT-induced H/J behavior extends beyond the perturbative limit, we show in Figure 6 the spectra corresponding to Figures 5c and 5d when the diabatic Frenkel and CT bands are tuned to resonance, $E_{CT} = E_{S_1}$. When $t_e = t_h$ (Figure 6a), two absorption bands emerge as oscillator strength is now shared evenly by the upper and lower exciton bands. In stark contrast, only a single band is observed when $t_e = -t_h$ (Figure 6b). These behaviors can be understood from the band dispersion in eq 9, which in the limit of $E_{CT} = E_{S_1}$ and $J_{Coul} = 0$ reduces to
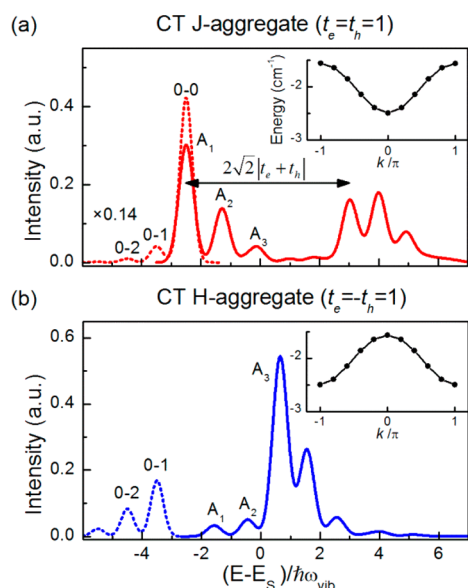
Figure 6. Absorption (solid) and PL (dashed) spectra for the (a) CT J-aggregate and (b) CT H-aggregate parametrized as in Figure 5 but with $E_{CT} - E_{S_1} = 0$. Insets show the dispersion curves for the lowest energy band.

$$E_{\pm}(k) = E_{CT} \pm \sqrt{2(t_e^2 + t_h^2 + 2t_e t_h \cos k)} \qquad (11)$$

Hence, the splitting of the bright exciton ($k = 0$),

$$|E_+(k = 0) - E_-(k = 0)| = 2\sqrt{2}|t_e + t_h| \qquad (12)$$

is much larger when t_e and t_h are in phase versus out of phase, an effect emphasized by Gisslen and Scholtz.[40] Figure 6a indicates that the splitting (double-headed arrow) remains essentially unchanged in the presence of vibronic coupling. Interestingly, in Figure 6a, the lower band retains J-like behavior, as indicated by the positive band curvature (see inset), the red-shifted main absorption peak, and the enhanced spectral ratios (A_1/A_2 and $0-0/0-1$) relative to the monomer. Conversely, the aggregate in Figure 6b shows H-aggregate behavior as indicated by the negative band curvature (see inset), the blue-shifted absorption maximum, and the suppressed spectral ratios. In fact, the 0−0 PL peak completely vanishes.

IV. INTERFERENCE BETWEEN COULOMBIC AND CT-MEDIATED COUPLING

In this section, we explore the interesting situations that arise when both the Coulombic and CT-mediated interactions are simultaneously present with similar magnitudes; such circumstances allow for pronounced constructive or destructive interferences between the two coupling sources. An example of the latter occurs in the π-stacked nanopillars of 7,8,15,16-tetraazaterrylene (TAT),[26] where the opposing Coulomb and CT-mediated interactions yield a significantly reduced exciton bandwidth.[31] The so-called H- to J-aggregate transformation observed in several perylene systems[29,30] is another example where the interference impacts the photophysical response.

To describe all such situations, we introduce a two-letter notation such as hJ; the first letter indicates the nature of the Coulomb coupling as deduced from the curvature of the diabatic Frenkel band (negative for h, positive for j), while the second letter designates the nature of the CT-mediated

coupling, as deduced from the curvature of the Frenkel-dominated adiabatic (after Frenkel/CT mixing) exciton band when $J_{Coul} = 0$. In the perturbative limit, the latter is simply dictated by the sign of J_{CT} in eq 4 (which depends on the sign of $t_e t_h$ and $E_{CT} - E_{S_1}$), while in the strong coupling limit, it depends only on the sign of $t_e t_h$, see eq 11. We use upper and lower case letters to indicate the relative magnitudes of the coupling strengths: in cases where the couplings are comparable, two upper-case letters are used. Hence, under the expanded notation, Kasha aggregates are designated as Jh, Jj, Hj, and Hh aggregates and the TAT nanopillars are HJ-aggregates (not to be confused with the polymer HJ-aggregates where the H- and J-couplings are segregated[7]).

Figure 7a demonstrates the interplay between the Coulomb and CT-mediated couplings occurring in hJ-aggregates ($J_{Coul} >$
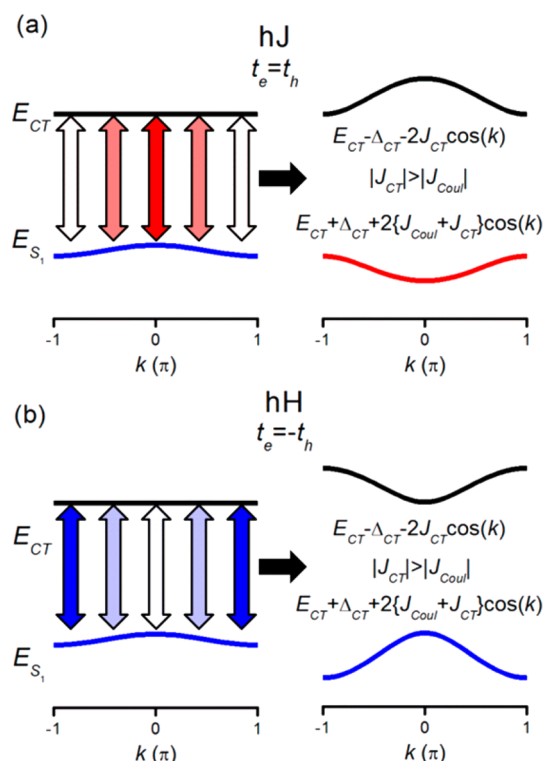

Figure 7. Formation of (a) hJ and (b) hH aggregates in the perturbative limit. In both cases, the Coulomb coupling predicts (Kasha) H-aggregates. Activation of Frenkel/CT coupling reverses the lower exciton band curvature in panel (a) while reinforcing it in panel (b).

0, $J_{CT} < 0$, $|J_{Coul}| < |J_{CT}|$) where the Frenkel/CT mixing is treated perturbatively. The diabatic Frenkel band in Figure 7a has a negative curvature due to the H-like Coulomb coupling. However, activating Frenkel/CT coupling with $|J_{CT}| > |J_{Coul}|$ causes a reversal of the band curvature; the resulting aggregate behaves photophysically like a J-aggregate. In a similar manner one could also envision a jH aggregate, where Coulomb coupling predicts a J-aggregate but the photophysics are H-like due to the dominant CT-mediated coupling.

In hH aggregates, both couplings are positive and reinforce each other, as demonstrated in Figure 7b. As in Figure 7a, the diabatic Frenkel band has negative curvature. However, when short-range coupling ($J_{CT} > 0$) is activated, the band curvature increases significantly resulting in more pronounced H-like
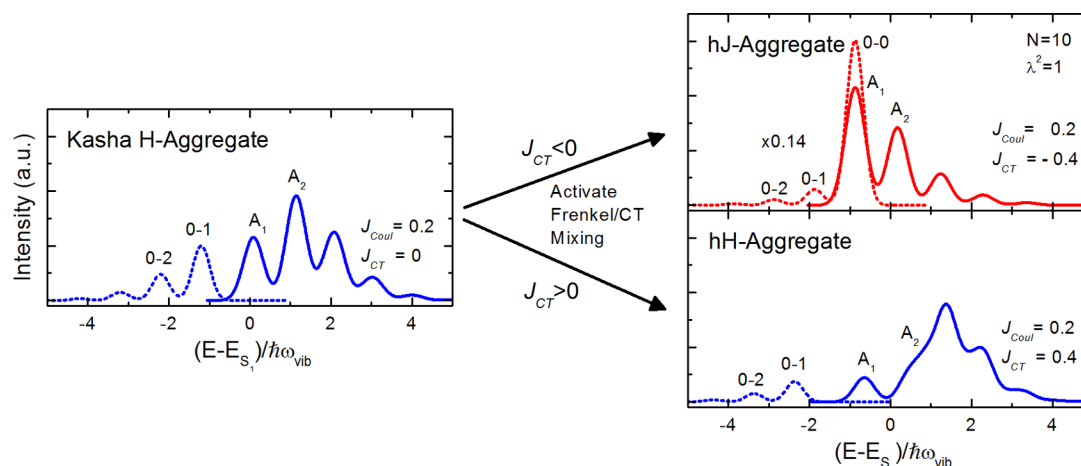
Figure 8. (left) Absorption and PL spectra for a Kasha H-aggregate with $J_{Coul} = 0.2$. Activating the CT integrals with $t_e = t_h = \sqrt{2}$ and $E_{CT} - E_{S_1} = 10$ results in J-aggregate photophysics (top, right). Taking $t_e = -t_h = \sqrt{2}$ gives reinforced H-aggregate behavior (bottom, right). All energies are in units of $\hbar\omega_{vib}(=1400 \text{ cm}^{-1})$. The HR factors are $\lambda^2 = 2\lambda_{\pm}^2 = 1$.
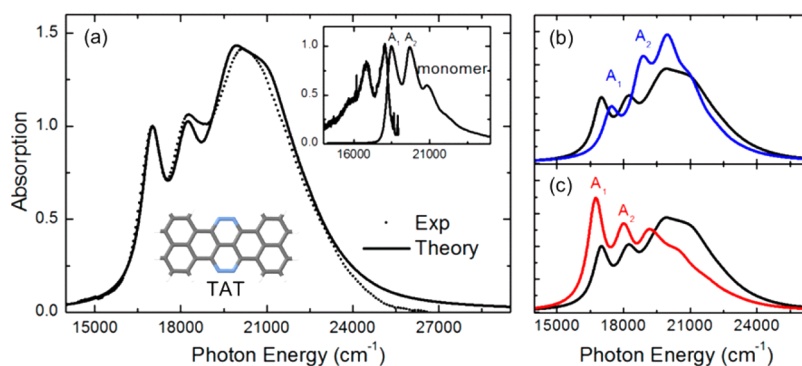

Figure 9. (a) The calculated absorption spectrum (solid line) for a π-stack containing 20 TAT molecules plotted against the measured spectrum (dotted line) of TAT nanopillars on graphene from ref 25 (see ref 26 for details). Right inset shows absorption and PL spectra for 100 nM TAT dissolved in chloroform. (b) Calculated spectrum excluding charge transfer ($t_e = t_h = 0$) but retaining extended Coulombic couplings (blue). (c) Calculated spectrum excluding Coulomb coupling but retaining charge transfer (red).

behavior. The spectral consequences of the destructive and constructive interferences present in hJ and hH aggregates are demonstrated in Figure 8.

Opposing CT-mediated (J-like) and Coulomb-mediated (H-like) behavior has recently been revealed in TAT nanopillars.[26] Figure 9 compares the measured and calculated absorption spectra for a 20-chromphore TAT π-stack (see ref 26 for details). The competition between the two coupling sources is revealed in Figures 9b and 9c where the CT and Coulomb couplings have been alternately turned off. When Frenkel/CT mixing is neglected (Figures 9b), the spectrum displays all of the attributes of a conventional Kasha H-aggregate due to the positive Coulombic couplings arising from the mainly side-by-side packing. By contrast, setting all Coulomb couplings to zero results in a spectrum characteristic of a classic J-aggregate (Figure 9c) but due entirely to CT-mediated short-range coupling. Interestingly, the measured A_1/A_2 ratio (Figure 9a) is essentially unchanged from that corresponding to monomeric TAT in solution indicating that the two destructively interfering coupling sources are comparable in magnitude, in excellent agreement with theory. Hence, the TAT nanopillars are HJ-aggregates. Subsequent calculations[31] showed that a transverse slip as small as ~0.5 Å changes the relative phase between the electron and hole integrals, effectively creating an HH-aggregate with profound physical consequences: The A_1/A_2

ratio plummets to approximately 1/3, indicative of strong H-aggregation, and the exciton bandwidth increases 3-fold resulting in a substantial increase in exciton mobility.[31]

Another example illustrating the intricate interplay of Coulombic and CT mediated interactions involves the so-called "H to J"-aggregate transformation observed in certain perylene derivatives.[29,30] Figure 10a shows the spectra corresponding to the H- and J-aggregate forms of a PBI–melamine complex from ref 29 along with the monomer in solution. The reversible transformation between H- and J-aggregate forms is associated with a change in the packing geometry due to the incorporation of a cyanuric acid derivative that changes the intermolecular hydrogen bonding pattern.[29] The theoretical simulations[44] shown in Figure 10b are based on two intermolecular packing geometries that correspond to two ground state minima of a perylene bisimide dimer as calculated by Fink et al. using DFT.[50] The simulated spectrum for the H-form is consistent with the minimum at (1.5 Å, 1 Å) where the two coordinates refer to the interperylene slip along the long- and short-axes, respectively. At this geometry, the CT integrals are weak, resulting in a spectrum that can be well described as a conventional H-aggregate. In contrast, the J-form, which is characterized by a spectrum with two broad peaks, is well-accounted for by assuming a configuration consistent with the second minimum at (3.0 Å, 0.8 Å), displaced by only 1.5 Å
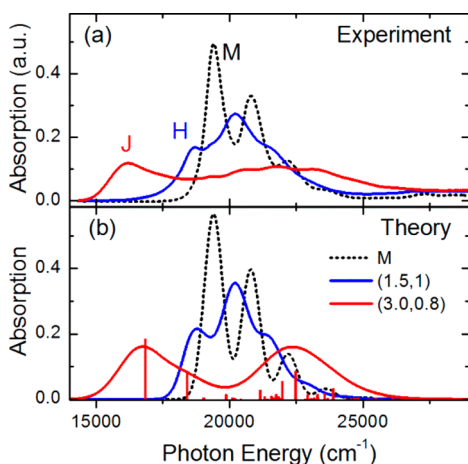
Figure 10. (a) Measured absorption spectra for the monomer in solution (M) and the J- and H-aggregated forms of the PBI−melamine complexes from ref 29. (b) Simulated spectra for a monomer in solution (black dash) and π-stacks of perylene chromophores at different stacking geometries, as noted in the figure legend, corresponding to the contour plots in Figure 4. The calculated stick spectrum for the J-form is also shown. Further details can be found in ref 44.

along the long molecular axis relative to the H-form. As Figure 4 demonstrates, this small packing change is enough to greatly amplify the *in-phase* charge-transfer integrals and convert the system into an hJ-aggregate. By contrast, Kasha's theory, based solely on Coulomb coupling, predicts H-like photophysics for the (3.0 Å, 0.8 Å) orientation (see Figure 4f). The J-form is an example of a J-aggregate with an unconventional geometry.

V. CONCLUSION AND OUTLOOK: DESIGNING ORGANIC MATERIALS

The general model for H- and J-aggregates outlined above can be exploited for the design of organic materials in a straightforward manner. For example, ideal absorbing materials for solar cell applications need to rapidly transport energy to the charge-transfer interface with minimal radiative loss. For such applications, one would prefer maximal exciton coupling between chromophores with little probability for emission, as in H-dominated aggregates (HH, Hj, jH). Conversely, materials for OLED applications would need to be highly emissive and highly conductive, as in JJ or Jh aggregates. Interestingly, high charge mobility and strong photoluminescence are often viewed as mutually exclusive properties, but there is no physical basis for this. Recently Liu et al.[51] reported high mobility, strongly emissive crystals of 2,6-diphenylanthracene with dominant J-like photophysics, consistent with the theory presented here.

The interference between J_{CT} and J_{Coul} is most pronounced when the two coupling sources are close in magnitude. In such cases, even sub-Å changes in the relative transverse orientation can reverse the sign of the CT-mediated coupling, substantially impacting the photophysical and transport properties, as recently demonstrated in TAT.[31] Such changes should be possible through chemical modification of the peripheral groups or through the application of a shearing force.[52] In designing such materials, deleterious factors such as thermal fluctuations,[47] site disorder, and excimer trapping[45,50] are serious considerations. However, interference effects in TAT were shown to be robust to fluctuations in J_{CT} on the order of

its mean value (-290 cm^{-1}) as well as to Gaussian site disorder distributed over several hundred wave numbers.[31]

The strong link between photophysical properties and transport properties also allows for efficient screening assays, which can take advantage of the large database already assembled for perylene derivatives. For example, the divergence of the A_1/A_2 ratio from the monomer value signifies a substantial exciton bandwidth; an increase (decrease) indicates J-type (H-type) materials. Moreover, in perylene monoimide nanoribbons the extent of electron and hole separation (and the resulting utility as photocatalytic scaffolds for hydrogen generation) can be obtained directly from the two-band absorption line shape.[49] In general, simple optical probes like steady-state absorption and photoluminescence contain a great deal of information about intermolecular coupling, a theme pioneered by Kasha for Coulomb-coupled ensembles and extended here to include short-range, CT mediated interactions.

■ AUTHOR INFORMATION

Corresponding Author

*E-mail: spano@temple.edu.

ORCID ⓘ

Frank C. Spano: 0000-0003-3044-6727

Notes

The authors declare no competing financial interest.

Biographies

Nicholas J. Hestand earned B.S. degrees in Chemistry and Mathematics from Evangel University in Springfield, Missouri, in 2012. He is currently a graduate student working with Dr. Spano.

Frank C. Spano received his Ph.D. in Chemistry from Princeton University in 1988. He is a professor in the Department of Chemistry at Temple University.

■ REFERENCES

(1) Reineke, S.; Thomschke, M.; Lüssem, B.; Leo, K. White organic light-emitting diodes: Status and perspective. *Rev. Mod. Phys.* **2013**, *85*, 1245−1293.

(2) *Organic Light-Emitting Diodes (OLEDs): Materials, Devices and Applications*; Buckley, A., Ed.; Woodhead Publishing: Cambridge, U.K., 2013.

(3) *The WSPC Reference on Organic Electronics: Organic Semiconductors*; Bredas, J.-L., Marder, S. R., Ed.; World Scientific Publishing Co: Singapore, 2016.

(4) Ostroverkhova, O. Organic Optoelectronic Materials: Mechanisms and Applications. *Chem. Rev.* **2016**, *116*, 13279−13412.

(5) Clarke, T. M.; Durrant, J. R. Charge Photogeneration in Organic Solar Cells. *Chem. Rev.* **2010**, *110*, 6736−6767.

(6) Bardeen, C. J. The Structure and Dynamics of Molecular Excitons. *Annu. Rev. Phys. Chem.* **2014**, *65*, 127−148.

(7) Spano, F. C.; Silva, C. H- and J-Aggregate Behavior in Polymeric Semiconductors. *Annu. Rev. Phys. Chem.* **2014**, *65*, 477.

(8) Bredas, J. L.; Beljonne, D.; Coropceanu, V.; Cornil, J. Charge-transfer and energy-transfer processes in pi-conjugated oligomers and polymers: A molecular picture. *Chem. Rev.* **2004**, *104*, 4971−5003.

(9) Schroter, M.; Ivanov, S. D.; Schulze, J.; Polyutov, S. P.; Yan, Y.; Pullerits, T.; Kuhn, O. Exciton-vibrational coupling in the dynamics and spectroscopy of Frenkel excitons in molecular aggregates. *Phys. Rep.* **2015**, *567*, 1−78.

(10) Coropceanu, V.; Cornil, J.; da Silva Filho, D. A.; Olivier, Y.; Silbey, R.; Bredas, J. L. Charge transport in organic semiconductors. *Chem. Rev.* **2007**, *107*, 926–952.

(11) Scholes, G. D.; Rumbles, G. Excitons in nanoscale systems. *Nat. Mater.* **2006**, *5*, 683–696.

(12) Spano, F. C. Excitons in conjugated oligomer aggregates, films, and crystals. *Annu. Rev. Phys. Chem.* **2006**, *57*, 217–243.

(13) Spano, F. C. The Spectral Signatures of Frenkel Polarons in H- and J-Aggregates. *Acc. Chem. Res.* **2010**, *43*, 429–439.

(14) Kasha, M.; Rawls, H. R.; El-Bayoumi, M. A.: *The Exciton Model in Molecular Spectroscopy*. Butterworths: London, 1965; Vol. *11*, pp 371–392.

(15) Kasha, M. Energy Transfer Mechanisms and the Molecular Exciton Model for Molecular Aggregates. *Radiat. Res.* **1963**, *20*, 55–70.

(16) Hochstrasser, R. M.; Kasha, M. Application of the exciton model to monomolecular lamellar systems. *Photochem. Photobiol.* **1964**, *3*, 317–331.

(17) Daltrozzo, E.; Scheibe, G.; Gschwind, K.; Haimerl, F. Structure of J-Aggregates of Pseudoisocyanine. *Photogr. Sci. Eng.* **1974**, *18*, 441–450.

(18) Kopainsky, B.; Hallermeier, J. K.; Kaiser, W. The 1st Step of Aggregation of Pic - the Dimerization. *Chem. Phys. Lett.* **1981**, *83*, 498–502.

(19) Würthner, F.; Kaiser, T. E.; Saha-Möller, C. R. J-Aggregates: From Serendipitous Discovery to Supramolecular Engineering of Functional Dye Materials. *Angew. Chem., Int. Ed.* **2011**, *50*, 3376–3410.

(20) *J-aggregates*; Kobayashi, T., Ed.; World Scientific: Singapore, 1996; p 228.

(21) Eisele, D. M.; Knoester, J.; Kirstein, S.; Rabe, J. P.; Vanden Bout, D. A. Uniform exciton fluorescence from individual molecular nanotubes immobilized on solid substrates. *Nat. Nanotechnol.* **2009**, *4*, 658–663.

(22) Ghosh, S.; Li, X.-Q.; Stepanenko, V.; Wurthner, F. Control of H- and J-Type p Stacking by Peripheral Alkyl Chains and Self-Sorting Phenomena in Perylene Bisimide Homo- and Heteroaggregates. *Chem. - Eur. J.* **2008**, *14*, 11343–11357.

(23) Harcourt, R. D.; Ghiggino, K. P.; Scholes, G. D.; Speiser, S. On the origin of matrix elements for electronic excitation (energy) transfer. *J. Chem. Phys.* **1996**, *105*, 1897–1901.

(24) Dexter, D. L. *J. Chem. Phys.* **1953**, *21*, 836.

(25) Wise, A. J.; Zhang, Y.; Fan, J.; Wudl, F.; Briseno, A. L.; Barnes, M. D. Spectroscopy of discrete vertically oriented single-crystals of n-type tetraazaterrylene: understanding the role of defects in molecular semiconductor photovoltaics. *Phys. Chem. Chem. Phys.* **2014**, *16*, 15825–15830.

(26) Yamagata, H.; Maxwell, D. S.; Fan, J.; Kittilstved, K. R.; Briseno, A. L.; Barnes, M. D.; Spano, F. C. HJ-Aggregate Behavior of Crystalline 7,8,15,16-Tetraazaterrylene: Introducing a New Design Paradigm for Organic Materials. *J. Phys. Chem. C* **2014**, *118*, 28842–28854.

(27) Fan, J.; Zhang, L.; Briseno, A. L.; Wudl, F. Synthesis and Characterization of 7,8,15,16-Tetraazaterrylene. *Org. Lett.* **2012**, *14*, 1024–1026.

(28) Gregg, B. A.; Kose, M. E. Reversible Switching between Molecular and Charge Transfer Phases in a Liquid Crystalline Organic Semiconductor. *Chem. Mater.* **2008**, *20*, 5235–5239.

(29) Yagai, S.; Seki, T.; Karatsu, T.; Kitamura, A.; Würthner, F. Transformation from H- to J-aggregated perylene bisimide dyes by complexation with cyanurates. *Angew. Chem., Int. Ed.* **2008**, *47*, 3367–3371.

(30) Sarbu, A.; Biniek, L.; Guenet, J.-M.; Mesini, P. J.; Brinkmann, M. Reversible J- to H-aggregate transformation in thin films of a perylenebisimide organogelator. *J. Mater. Chem. C* **2015**, *3*, 1235–1242.

(31) Hestand, N. J.; Tempelaar, R.; Knoester, J.; Jansen, T. L. C.; Spano, F. C. Exciton mobility control through sub-angstrom packing modifications in molecular crystals. *Phys. Rev. B: Condens. Matter Mater. Phys.* **2015**, *91*, 195315.

(32) Thompson, A. L.; Gaab, K. M.; Xu, J.; Bardeen, C. J.; Martinez, T. J. Variable Electronic Coupling in Phenylacetylene Dendrimers: The Role of Forster, Dexter, and Charge-Transfer Interactions. *J. Phys. Chem. A* **2004**, *108*, 671–682.

(33) Davydov, A. S. *Theory of Molecular Excitons*; Plenum: New York, 1971.

(34) Beljonne, D.; Cornil, J.; Silbey, R.; Millie, P.; Bredas, J. L. Interchain interactions in conjugated materials: the exciton model versus the supermolecular approach. *J. Chem. Phys.* **2000**, *112*, 4749–4758.

(35) Gierschner, J.; Park, S. Y. Luminescent distyrylbenzenes: tailoring molecular structure and crystalline morphology. *J. Mater. Chem. C* **2013**, *1*, 5818–5832.

(36) Bialas, D.; Zitzler-Kunkel, A.; Kirchner, E.; Schmidt, D.; Wurthner, F. Structural and quantum chemical analysis of exciton coupling in homo- and heteroaggregate stacks of merocyanines. *Nat. Commun.* **2016**, *7*, 12949.

(37) Merrifield, R. E. Ionized states in a one-dimensional molecular crystal. *J. Chem. Phys.* **1961**, *34*, 1835–1839.

(38) Hoffmann, M.; Schmidt, K.; Fritz, T.; Hasche, T.; Agranovich, V. M.; Leo, K. The lowest energy Frenkel and charge-transfer excitons in quasi-one-dimensional structures: application to MePTCDI and PTCDA crystals. *Chem. Phys.* **2000**, *258*, 73–96.

(39) Hoffmann, M.; Soos, Z. G. Optical absorption spectra of the Holstein molecular crystal for weak and intermediate electronic coupling. *Phys. Rev. B: Condens. Matter Mater. Phys.* **2002**, *66*, 024305.

(40) Gisslen, L.; Scholz, R. Crystallochromy of perylene pigments: Interference between Frenkel excitons and charge-transfer states. *Phys. Rev. B: Condens. Matter Mater. Phys.* **2009**, *80*, 115309.

(41) Smith, M. B.; Michl, J. Singlet Fission. *Chem. Rev.* **2010**, *110*, 6891–6936.

(42) Kazmaier, P. M.; Hoffmann, R. A theoretical study of crystallochromy-quantum interference effects in the spectra of perylene pigments. *J. Am. Chem. Soc.* **1994**, *116*, 9684–9691.

(43) Yamagata, H.; Pochas, C. M.; Spano, F. C. Designing J- and H-aggregates through wave function overlap engineering: applications to poly(3-hexylthiophene). *J. Phys. Chem. B* **2012**, *116*, 14494–14503.

(44) Hestand, N. J.; Spano, F. C. Interference between Coulombic and CT-mediated couplings in molecular aggregates: H- to J-aggregate transformation in perylene-based pi-stacks. *J. Chem. Phys.* **2015**, *143*, 244707.

(45) Schubert, A.; Settels, V.; Liu, W.; Würthner, F.; Meier, C.; Fink, R. F.; Schindlbeck, S.; Lochbrunner, S.; Engels, B.; Engel, V. Ultrafast Exciton Self-Trapping upon Geometry Deformation in Perylene-Based Molecular Aggregates. *J. Phys. Chem. Lett.* **2013**, *4*, 792–796.

(46) Margulies, E. A.; Miller, C. E.; Wu, Y.; Ma, L.; Schatz, G. C.; Young, R. M.; Wasielewski, M. R. Enabling singlet fission by controlling intramolecular charge transfer in π-stacked covalent terrylenediimide dimers. *Nat. Chem.* **2016**, *8*, 1120–1125.

(47) Aragó, J.; Troisi, A. Dynamics of the Excitonic Coupling in Organic Crystals. *Phys. Rev. Lett.* **2015**, *114*, 026402.

(48) Yamagata, H.; Norton, J.; Hontz, E.; Olivier, Y.; Beljonne, D.; Bredas, J. L.; Silbey, R. J.; Spano, F. C. The nature of singlet excitons in oligoacene molecular crystals. *J. Chem. Phys.* **2011**, *134*, 204703.

(49) Hestand, N. J.; Kazantsev, R. V.; Weingarten, A. S.; Palmer, L. C.; Stupp, S. I.; Spano, F. C. Extended-Charge-Transfer Excitons in Crystalline Supramolecular Photocatalytic Scaffolds. *J. Am. Chem. Soc.* **2016**, *138*, 11762–11774.

(50) Fink, R. F.; Seibt, J.; Engel, V.; Renz, M.; Kaupp, M.; Lochbrunner, S.; Zhao, H. M.; Pfister, J.; Wurthner, F.; Engels, B. Exciton trapping in pi-conjugated materials: A quantum-chemistry-based protocol applied to perylene bisimide dye aggregates. *J. Am. Chem. Soc.* **2008**, *130*, 12858.

(51) Liu, J.; Zhang, H. T.; Dong, H. L.; Meng, L. Q.; Jiang, L. F.; Jiang, L.; Wang, Y.; Yu, J. S.; Sun, Y. M.; Hu, W. P.; Heeger, A. J. High mobility emissive organic semiconductor. *Nat. Commun.* **2015**, *6*, 10032.

(52) Giri, G.; Verploegen, E.; Mannsfeld, S. C. B.; Atahan-Evrenk, S.; Kim, D. H.; Lee, S. Y.; Becerril, H. A.; Aspuru-Guzik, A.; Toney, M. F.;

Bao, Z. A. Tuning charge transport in solution-sheared organic semiconductors using lattice strain. *Nature* **2011**, *480*, 504−U124.